Scaling behaviors of colloidal aggregates under uniform pressure

Robert Botet[1] and Bernard Cabane[2]
[1]*Laboratoire de Physique des Solides, CNRS / Université Paris–Sud, Centre d'Orsay, Bâtiment 510, F-91405 Orsay, France*
[2]*Laboratoire PMMH, ESPCI, 10 Rue Vauquelin, F-75231 Paris Cedex 05, France*
(Received 1 April 2004; published 29 September 2004)

We present a theoretical model for the compaction of a colloidal sediment under uniaxial mechanical pressure in the continuous three-dimensional space. The initial system is formed with aggregated particles dispersed in a fluid, and softly sedimented in a vessel. When a uniform pressure is applied, it evolves irreversibly through successive creation and destruction of bonds between the particles. The rules governing the bonds depend on both geometrical constraints and current stresses. Numerical simulations of such systems exhibit three different scenarios, corresponding, respectively, to the fragile, elastic, and plastic behaviors. In the elastic regime, where most bonds are permanent, the pressure scales as a power law of the volume fraction of particles, with a numerical exponent equal to 4.4. In the plastic regime, where many bonds are broken and many others created, the pressure also scales with volume fraction, but the exponent is much lower, equal to 1.7. These scaling behaviors agree remarkably well with recent experiments realized on the compaction of systems with aggregated silica particles in the œdometer cell. They also can be explained with simple theoretical arguments using a plausible morphology of the resistant paths acting throughout the system. Finally, at very large applied pressures, all these regimes converge to the random close packing of spheres.

DOI: 10.1103/PhysRevE.70.031403 PACS number(s): 83.80.Hj, 05.20.Gg, 05.70.Fh, 05.50.+q

I. INTRODUCTION

This paper deals with the behavior of disordered networks, such as those formed by aggregated colloidal particles, when they are submitted to a compressive force. From a fundamental point of view, the question of the compression of an N-body system takes place in a number of physical contexts. A classical example is the problem of gas compression under the uniform pressure. It has been solved for a long time, after considering the gaseous medium as a disordered ensemble of molecules in thermal equilibrium. For the ideal gas, the resistance to collapse comes from the kinetic energies of the molecules, and this results in very particular laws for the pressure P versus the gas density ϕ. Importantly, these laws depend on the precise way in which the gas is compressed. For example, Boyle's law is the elastic behavior: $P \propto \phi$ for the isothermal transformation. The control of energy, instead of control of temperature, leads to different behaviors, as Poisson's law: $P \propto \phi^{\gamma}$, with $\gamma = 1.3-1.7$ for the reversible adiabatic compression. Such power-law behaviors, as

$$P \propto \phi^{1+1/n}, \tag{1}$$

with the real positive polytropic index n, are common for perfect-gas compression. Deviations to these laws appear when interactions between molecules arise. The two-bodies attractive intermolecular forces tend to decrease the real pressure by a quantity proportional to ϕ^2. Moreover, the finite volume of the molecules must manifest at the very large densities, leading to the Van der Waals equation

$$P + a\phi^2 \propto \phi/(\phi^* - \phi) \tag{2}$$

for the isothermal case, with ϕ^* the limit density at the infinite pressure. These considerations are general, and should hold for any disordered system of particles that interact through central forces. However, in colloidal systems, particles often interact through noncentral forces. This is the case for all colloidal aggregates, in which small particles are held together by surface forces. Because such forces are noncentral, they may cause the aggregates to retain tenuous or bushy structures, as in the case for fractal aggregates [1]. All colloidal pastes, such as ceramic pastes and flocculated emulsions, are made of such aggregates that form a network extending throughout the material. It would be highly desirable to be able to predict, from the knowledge of interparticle forces, the response of such networks to an applied strerss.

In this paper, we propose a study of the quasistatic isothermal mechanical compression of an inhomogeneous network of colloidal particles. We consider the case where colloidal particles interact through local chemical bonds, yielding aggregation, and eventually Van der Waals and screened electrostatic forces. In the chemical engineering language, this system would be called a paste. Specifically, the colloid aggregates may be placed in a compression cell, as in a colloidal ultrafiltration experiment where a semipermeable piston expresses the liquid from a paste. Quasistaticity means here that the characteristic compression time is much larger than the relaxation time of the overall structure. Within this framework, the compressive yield stress is expected to be a material property of the colloidal system.

Following the ideas for the granular matter packing [2], the forces propagate along particular paths of connected particles, and these paths are responsible for the relevant mechanical behavior of the whole system through the local stress distribution. The local mechanisms involved in the irreversible deformation of the system, are then creation, deformation, and breaks of the bonds between the colloidal particles. The bonds originate from the surfaces of the particles, and therefore produce *noncentral* forces, hence the network resists bending deformations and will not collapse spontaneously. Therefore, bond-stretching deformations re-

sult in the elastic response to applied forces, while the irreversible events give the plastic response at high deformation of the network. For the latter, bond creations and breaks are expected to occur mainly following avalanches of complex events involving rupture, reordering, and creation, until mechanical equilibrium is reached. Even if alternative behaviors have been proposed [3,4], the power laws for the pressure versus volume fraction are commonly used in this context [5].

In Sec. II, we present new modeling of the compaction of aggregated solid spheres with creation/annihilation of harmonic springs representing the total interaction between spheres. In Sec. III, a simple theoretical model is described, and the various power laws between pressure and volume fraction, predicted by this model, are drawn. A discussion of the numerical data and a comparison with the theoretical model are presented in Sec. IV.

II. NUMERICAL MODEL

The model proposed here is a variant of the discrete element method [6] — used for granular materials — in which each particle is regarded as an individual hard element, and actual microscopic forces result from pair interactions. We consider a box of linear dimension $L_x \times L_y \times L_z$, the finite part of the continuous three-dimensional space, and, at the beginning of each simulation, N spherical particles are dispersed into this box under preaggregated forms. The common radius of the particles is $a=1/2$, such that $2a$ defines the natural unit of length: the values of all lengths will be defined relatively to $2a$.

In the current work, we shall take the values: $L_x=L_y=11$, and the height L_z in the range 11–200. The z axis defines the direction of the external pressure forces. The colloidal particles are all inside the region $z=0$ and H, with H the sediment height, which is essentially a decreasing function of the pressure. Along the x and y directions, periodic boundary conditions are considered.

The common mass of the particles is set to 1, and each particle is allowed to translate and rotate according to the laws of classical mechanics.

A. Definition of the pins

At the beginning of each simulation, a series of pins is randomly computed for each particle. A pin is a particular point of the *surface* of the sphere, where a bond may be attached. Only one bond can catch a given pin at the same time. Hereafter, the number n_t of such pins per sphere will be fixed to 200, unless duly noticed. This means that it is not possible to attach more than 200 bonds onto the surface of a sphere (excluded volume effect). The relevance of the value given to this number is discussed in Sec. IV B.

The exact locations of the pins are computed following a Monte Carlo procedure: a point on the surface of a sphere is chosen randomly; it is accepted as a pin if the direction joining the center of the sphere to this new point makes an angle larger than a threshold with any other pins of the same sphere (e.g., 0.2 rad is a correct threshold to obtain $n_t=200$). The algorithm is repeated until the required number of pins is obtained. This insures a statistically uniform distribution of the pins on the surface. All these pins are fixed in a local frame attached to the particle. Indeed, during the movement of the particle, this local frame translates and rotates with respect to the global frame of the box.

B. Initial aggregates

Before applying the pressure, one builds the system by adding N particles to the box. We use the standard reaction-limited cluster-cluster aggregation (RCCA) model [1] to generate randomly aggregates of N_a identical particles. This model is known to correctly describe experimental flocculation of colloidal particles — such as silica [7], polystyrene [8], or metallic [9,10] colloids — in the conditions where the aggregation rate is limited by the time it takes by the clusters to form a bond.

All the results presented below have been obtained with $N_a=16$, but work is in progress with other values of N_a ranging from 1 to 32, in order to understand the role of the eventual preaggregation on the compacted structure. The $N=16$ RCCA aggregates correspond to an ensemble of fractal aggregates of fractal dimension $D_f=2$, and a radius of gyration $R_g/2a=2.2$ [11].

Once an aggregate is generated, it is inserted randomly at top of the box, at a height large enough to avoid any overlap with previous system particles. Whenever the aggregate is self-overlapping, due to the lateral periodic boundary conditions, single-bonded particles are removed one by one from this single aggregate until there is no more self-overlap. The remaining aggregate is then gently settled onto bottom of the box, or onto existing particles, without deformation of its structure. Overlaps are strictly forbidden at this stage. With the use of this algorithm, one adds as many particles as wished. Generally, the simulations presented hereafter were made with ~ 500 particles. Within the box of lateral section 11×11, this corresponds to an initial volume fraction for the sediment $\phi \approx 10^{-2}$.

C. Creation and annihilation of the bonds

Bonds are generated if the relative distance between two free pins belonging to two different spheres is smaller than a threshold l_a (see Fig. 1). Such a bond will link the two spheres by a microscopic massless spring of stiffness k, and characteristic length l_o. The two pins used for the bond cannot be used again as long as this bond is present.

The spring parameters k and l_o define the energy unit through the relation $E_o=kl_o^2/2$, which is the energy needed to compress a spring completely. The simulations presented here are done for the particular choice $l_a=l_o$. This means that no energy is gained or lost by the creation of a bond.

According to the forces acting on the particles, these springs can contract or stretch from their equilibrum length l_o. Whenever the length of the spring becomes larger than a threshold $l_{\max}$, the bond is destroyed (see Fig. 2), releasing the microscopic disruptive energy $E_d=k(l_{\max}-l_o)^2/2$ into the fluid. The value of the relative energy E_d/E_o is used to characterize the fragility of the system (not to be confused with

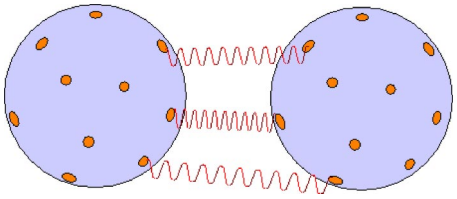

FIG. 1. A schematic view of two spheres connected by a few springs. Pins are marked as small gray chips on the surface of each sphere. Two bonds cannot attach to the same pin, and a given bond connects two different spheres. It is clear that such a configuration yields natural resistance to bending: when three or more springs are attached to the surface of two spheres — as on the figure — no relative movement of the spheres can be performed without changing the lengths of at least one spring. It results in bending forces.

the softness of the system, which is directly connected to the value of k). The fragility parameter ranges from 4×10^{-2} to 10^5 in the simulations presented below.

D. Soft core

The spheres are not considered as hard spheres, but overlaps are allowed within a shell of width $a/10$ according to prescription discussed in Ref. [12]. This results in a repulsive central harmonic force proportional to the overlap length. The stiffness constant is set equal to $10E_d/a^2$. In fact, the quantitative results did not depend on the precise value of the numerical coefficient, if it was chosen within the range 1–30.

E. Application of the external pressure

Several experimental situations have been considered (e.g., a system in a gradient of pressure, as in a centrifugation experiment), but here, we will focus only on the application of a uniform pressure, as in the experiment with a piston in the œdometer cell. If the current system is entirely inside a column of vertical extension $[0,H]$, then the external pressure P induces a pressure force $\pi a^2 P$ on any sphere intersecting the slices $0<z<a$ or $H-a<z<H$. The other spheres inside the system do not feel directly the pressure.

F. Dynamics

Once all the objects of the system and their applied forces have been defined, one has to consider the proper rules for the individual motions. A particle, say i, is submitted to various forces, the sum of which is noted $\vec{F}_i$. They can be split into two sets: the central forces (the pressure force and the overlapping forces), and the noncentral forces (forces due to the bonds, which are attached to the surface of the particle). The latter generate moments, the sum of which is $\vec{M}_i$, which tend to rotate the particles. The equations of motion in the frame of the box are

$$m\frac{d\vec{v}_i}{dt} = \vec{F}_i + \lambda(\vec{v}_f - \vec{v}_i),$$

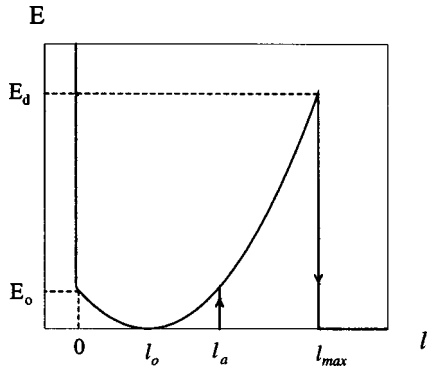

FIG. 2. Sketch of the mechanical potential energy E of a bond vs the separation distance l between the surfaces of two spheres facing each other. The bond equilibrium length is l_o. For two spheres approaching, a bond is created at the distance l_a (for clarity, the figure is drawn for the case $l_a>l_o$, but the simulations presented in the work are for $l_a=l_o$). The value E_o of the potential energy for $l=0$ defines the unit of energy in the system. Small negative values of the length l are possible, but they correspond to rapidly increasing repulsive forces. For two spheres moving away, the bond is destroyed at the distance l_{max}. The value E_d of the potential energy at this rupture threshold characterizes the fragility of the system.

$$\frac{5}{2}ma^2\frac{d\vec{\omega}_i}{dt} = \vec{M}_i + \frac{4}{3}a^2\lambda(\vec{\omega}_f - \vec{\omega}_i),$$

where $\vec{v}_i$ and $\vec{\omega}_i$ denote the current translational and angular velocity of particle i, while $\vec{v}_f$ and $\vec{\omega}_f$ are the corresponding macroscopic velocities of the fluid at the location of particle i. The coefficient λ is the proportionality constant between the drag force on a particle and its relative translational velocity with respect to the fluid in the Stokes regime.

In principle, one has to deduce the position and orientation of particle i by the time integration of $\vec{v}_i$ and $\vec{\omega}_i$. This should be done using (e.g.,) the Verlet algorithm with implicit velocity [13], to compute the new position of the particle at time $t+\delta t$, knowing its position at times t and $t-\delta t$, and the local forces $\vec{F}_i$ (pressure and spring forces) and $\lambda\vec{v}_f$ (drag forces). This would require complete knowledge of the fluid velocity field $\vec{v}_f$, which is a considerable task. Instead, we will consider that all velocities appear to be small (quasistatic approximation), therefore neglecting drag forces and moments. During the time interval δt, small enough for all the forces to be considered as constant, one has for the position $\vec{r}_i$ and orientation θ_i of the particle i

$$\delta\vec{r}_i = \alpha\vec{F}_i, \tag{3}$$

$$\delta\theta_i = \beta M_i, \tag{4}$$

with the coefficients $\alpha=(\delta t)^2/2m$ and $\beta=2\alpha/5a^2$. In Eq. (4), the rotation of angle $\delta\theta_i$ is around the axis $\vec{M}_i/M_i$.

This approximation is based on the fact that, at equilibrium (and we are interested by the equilibrium state of the stressed system), all the velocities vanish, fluid velocity included. So, drag forces do not play a relevant role close to equilibrium in the present situation. More quantitatively, ex-

pressing $\lambda = 6\pi\nu\rho_f a$, with ν the kinematic viscosity of the fluid of volumic mass ρ_f, and considering a fluid velocity of same order of magnitude as particle velocities, quasistatic condition $\lambda v_i \ll F_i$ writes here: $\nu\delta t/a^2 \ll 1$. This means that the characteristic time increment δt should be much smaller than the momentum diffusion time over distance a (typically $\sim 10^{-11}$s for colloidal particles in the water). We will not discuss further the definition of time through δt, but only consider the algorithm Eqs. (3) and (4) as a convenient way to determine the iso-static state $\{\vec{F}_i = \vec{0}, \vec{M}_i = \vec{0}\}_{i=1,\cdots,N}$ of the system, after a small increase of the external pressure.

G. Algorithm for evolution to a quasistatic equilibrium

The algorithm for time evolution is as follows: a given geometry and pressure being given, all the forces and moments are computed according to the foregoing rules detailed in Sec. II C–II E. The equations of motion (3) and (4) are then used successively on all the particles of the system, with the coefficient α chosen in such a way that the largest translational movement equals $a/10$. So, to optimize the simulation speed, the time is allowed not to run uniformly. After displacement of all the particles is achieved, the bonds are updated: some of them are broken apart and other ones appear, according to the Sec. II C rules. The same applies to the particles submitted to the external pressure, and to the overlaps. Once the whole geometry has been updated for one step time, one performs the loop again at the given constant pressure. The computer realizes as many loops as needed for the equilibrium be reasonably reached. To achieve this stop, one checks the displacements of all the particles. When the maximum and the average value of these displacements are both smaller than a threshold (namely, $a/100$) for 20 consecutive time steps, the simulation stops. Mechanical equilibrium is then considered achieved, and one increases the pressure. The full algorithm is then used once again.

III. ORDER OF MAGNITUDE OF THE VARIOUS PARAMETERS

The correct values of the parameters can be inferred from estimates of the fundamental quantities used in the model. Assume that the system is a colloidal dispersion, made of nanometric particles. The particle diameter may be taken as $2a = 6$ nm, and the equilibrium length of the spring as $l_o = 3$ nm. The natural pressure unit is $P_o = kl_o/\pi a^2 \equiv E_o/\pi a^3 (l_o/2a)$. To get P_o of order 1 bar, one can choose for the energy of a completely compressed spring: $E_o \approx 4 \times 10^{-21}$ J, which corresponds approximately to $1k_BT$ at room temperature. This will be our choice in the following: the values P/P_o will then be understood as effective pressure P expressed in bars, and the values of E/E_o as energy E expressed in k_BT units.

During a simulation, neighboring particles will be linked by several bonds connected to their surfaces. So, the mechanical response of the system will result from the properties of bundles of springs instead of individual bonds. Therefore, a quantity of interest is the energy needed to separate two particles linked together by the maximum number of springs. Putting two spheres into contact, the area of one sphere, at a distance less than l_a from the corresponding area of the other sphere, is $\pi a l_a$. The pins being uniformly distributed over the surface of the sphere, the number of bonds linking the two spheres is the product of the total number of pins per sphere with $l_a/4a$. For $n_t = 200$ pins per sphere, and $l_a = l_o$, one gets ten bonds between the two spheres in contact. The energy needed to completely separate the two spheres is then $10E_d$ in this case. It ranges from $0.04k_BT$ to $10^5 k_BT$ for the values of E_d investigated. Note also that, if two spheres are brought into contact, then released, the bundle of springs is equivalent to a single harmonic spring with local stiffness $K_o = kn_t\, l_a/4a$ at the equilibrium length $l_o - l_a/2$. A sketch of the force applied to the spheres versus the distance l separating their centers is shown in Fig. 3.

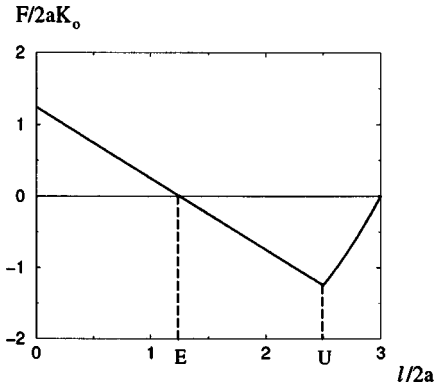

FIG. 3. A sketch of the reduced total force between two spheres initially in contact, versus their separation distance $l/2a$ during traction from particles in contact. Repulsive forces are counted positive. In this example, the parameters $l_a/2a = l_o/2a = 1/2$ and $l_{max}/2a = 2$ have been used. This corresponds to the disruptive parameter $E_d/E_o = 9$. When l is smaller than $l_U = 2a + l_{max} - l_a$ (noted U on the figure), interaction is elastic and harmonic. The equilibrium length is $l_E = l_o - l_a/2$ and equivalent stiffness K_o. When separation distance becomes larger than l_U, the system becomes unstable with respect to traction, as irreversible bond breaking occurs. The case exemplified here is typical of $l_a/2 < l_o < l_{\max}$. For the other cases (not considered in the paper), the two-sphere system is always repulsive (if $l_o > l_{max}$) or always attractive (if $l_o < l_a/2$) regardless the separation distance.

The largest force F_{max} that two spheres are able to generate in response to a separating stress, is such that $F_{max}/K_o l_o = \sqrt{E_d/E_o} - l_a/2l_o$ for the usual case $E_d/E_o > (l_a/l_o)^2$ [and $F_{max}/K_o l_o = E_d l_o/2l_a$ for the fragile case $E_d/E_o < (l_a/l_o)^2$]. It should be compared to the other characteristic force in the system: the pressure force. The whole structure is then unable to resist to the pressure if $F_{max} < \pi a^2 P$. This gives an order of magnitude of the largest pressure P^*_{dis} (disruptive pressure) that the system is able to support

$$P^*_{dis}/P_o = \frac{n_t}{2}\frac{l_a}{2a}\left(\sqrt{\frac{E_d}{E_o}} - \frac{l_a}{2l_o}\right). \tag{5}$$

For $P > P^*_{dis}$, the forces generated by the springs cannot balance the typical forces generated by the external pressure.

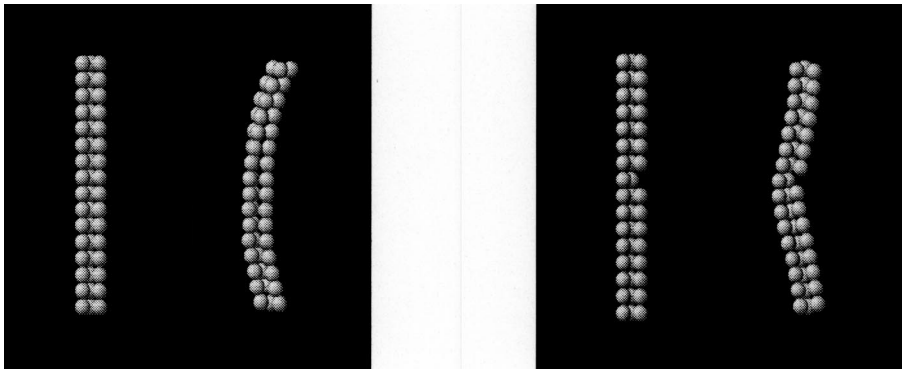

FIG. 4. Two examples of columns with a triangular basis are shown. The bonds between neighboring particles are created in the initial structure, and cannot be destroyed or created during deformation. (a) The two left-hand side columns show elastic twisting and buckling. (b) The two right-hand side columns show the folding of the column when a defect (one central particle is missing) is created in the initial structure.

The structure of the overall system is then expected to be completely destroyed until the hard-sphere repulsion forbids subsequent collapse.

IV. CHECKS

A number of test simulations have been performed in order to verify the relevance of the algorithm for modeling the deformation of multisphere bodies, with the correct choice of the dummy parameters.

A. Deformation of simple bodies

The algorithm, as stated in Sec. II G, could be used with minor changes, to study the elastic response of a multisphere body, connected by *permanent* bonds. In this case, the bonds are created once and for all at the beginning of the process, and they cannot be created or broken during the rest of the simulation.

A quantitative check was perfomed in this sense, on an ensemble of four particles in contact, arranged in the regular tetrahedron. The numerical results for its response to the uniform pressure, agree quantitatively well with the analytical result which is easy to derive because of the symmetry of the problem.

Another, less obvious, test is the response of a column squeezed between two pistons. In Fig. 4 are two examples of a cylindrical column with the triangular basis (i.e., formed initially by the regular vertical arrangement of ensembles of three particles, organized in equilateral triangles). As explained above, the bonds in this numerical experiment are permanent and cannot be created or broken during deformation, therefore, the response to external force must be purely elastic. On the first example [Fig. 4(a)], one sees the twisting and buckling of the structure. Twisting appears first as a response to small compression: triangles of particles rotate with respect to each other in order to decrease the overall height. When this process is no longer possible — or requires too much mechanical energy — the system buckles. In Fig. 4(b) the same column is shown after a central particle was removed. This generates a structural defect, and the system prefers to fold down. These two behaviors are indeed expected for the elastic response, if the forces propagate correctly throughout the structure.

B. Values of the dummy parameters

Other tests were performed to verify that the quantitative results are robust with respect to those parameters that are expected to be irrelevant. An example is given below, in Fig. 5, where simulations were realized with systems of $N=256$ or 512 particles, and particles with 200, 300, or 400 pins. The numerical results show the increase of the volume fraction with pressure.

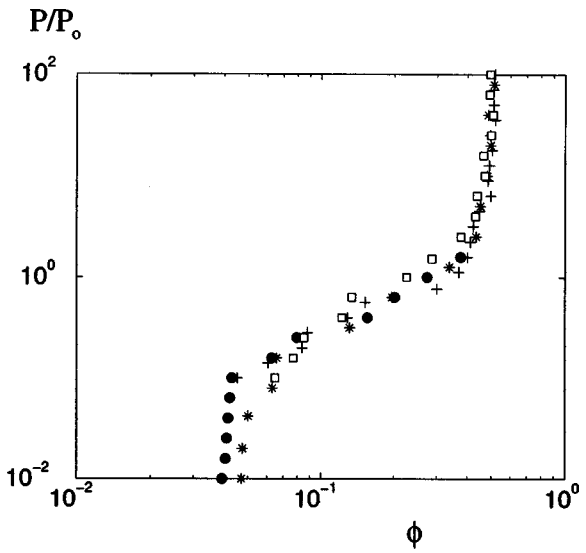

FIG. 5. Volume fraction vs pressure, for four different cases with the common value $E_d/E_o=1$. The stars are $N=256$ and $n_t=200$ pins per particle; crosses for $N=256$, $n_t=300$; squares for $N=256$, $n_t=400$; circles for $N=512$ and $n_t=400$ pins per particle. All the data fall on a single curve, which shows that the number of particles and the number of pins per particle are so large that they no longer noticeably influence the statistical results. The values for the disruptive pressures P^*_{dis}/P_o given by Eq. (5) are 25 for $n_t=200$ and 50 for $n_t=400$.

Except from the very initial stage (the initial sediments were different), the regular trend starting at the external pressure $P=0.1$ is similar for the four cases. One can then conclude that the values $N=256$ and $n_t=200$ are large enough to avoid any spurious dependence of the system size and of the number of possible bonds per particle. In the following, all numerical simulations were made with $N\approx 500$, and $n_t=200$.

An important remark must be made here: we see in Fig. 5 that the main global features do not depend on the initial conditions of the compression. This could be remarked in all the simulations presented below. This point suggests the existence of general scenarios governing the compressive behaviors of such systems. This will be the reason for the tentative outline chosen throughout this paper: to extract global behavior and propose general scenarios to explain them.

C. Increment of pressure

At this point, it is useful to make the following remark concerning the exponential increment of pressure. We use the following prescription: starting from a small value P_1, the pressure is increased by multiplying it successively by a constant factor. In such a way, the increment $\Delta \log P$ is constant. The reason for such a choice, is that the larger the pressure, the weaker the possible compaction of the system. In addition, this exponential scale is well adapted to detect power-law behaviors [like Eq. (1) for example]. Such a power law is apparent in Fig. 5 for pressures in between 0.1 and 2 bars.

The relevance of this choice has been checked using a linear, instead of exponential, increase of pressure, with various pressure steps. The results remain identical regardless of the increment, provided it is very much smaller than the pressure P^*_{dis} needed to completely collapse the system. In the example of Fig. 5, one should consider the increment of pressure to be much smaller than a few P_o (here, a few bars, since $P_o\sim 1$ bar). Applying, for example, $P_1=100$ bars as the first pressure would lead to a very inhomogeneous system, as a consequence of the basic irreversibility of the process. This process could be relevant in some fast experimental compression for which kinetics is expected to play an important role, but the time should then be handled very precisely in the numerical model. This is not the aim of the present paper, mainly devoted to quasistatic transformations.

D. Example

A sketch of the visual aspect of the particle system (the bonds are not represented), is shown in Fig. 6 for three successive pressures. These are projections onto the x-z plane, so the system appears more dense than it actually is. One can note that the system remains fairly homogeneous, which is a well-known result for the œdometer experiments.

V. THEORETICAL MODEL

We propose here a simple theoretical model able to catch the main behaviors found in our numerical simulations, which are presented in Sec. VI. It corresponds to an extreme simplification of the numerical model presented in Sec. II,

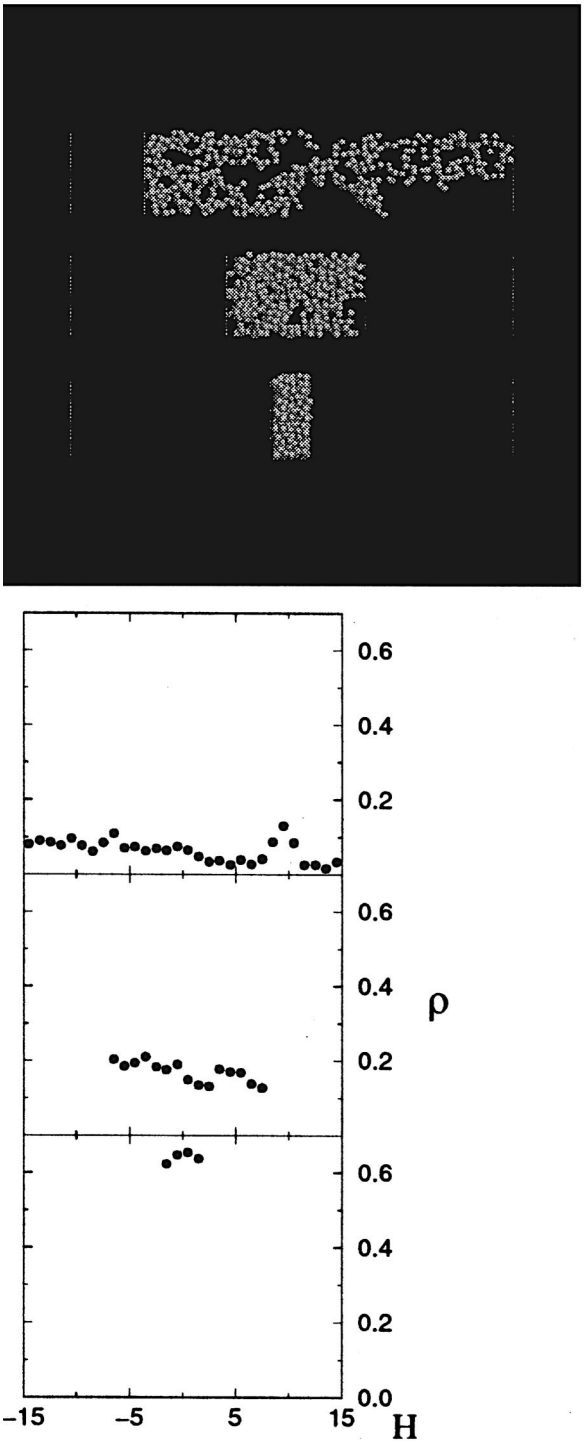

FIG. 6. Three pictures (projections) of the same system during compaction. The value of E_d/E_o is here equal to 4, and the number of particles is $N=500$. Volume fractions are, respectively, 0.06, 0.30, and 0.63 from top to bottom. The dashed lines visualize the initial and actual planes where external pressure is applied. Periodic boundary conditions are applied on all other sides. The curves at the right-hand side are the respective density profiles for the three cases. Except for small statistical fluctuations, the systems are spatially homogeneous.

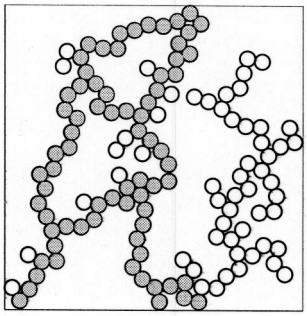

FIG. 7. A visualization of the mechanically resistant columns in a two-dimensional system made of eight aggregates of 16 disks. The aggregates are built one after the other by the general RCCA algorithm [1]. Once an aggregate is completed, it settles from top to bottom without deforming. There is just one resistant column (made of the gray particles) with loops.

and is discussed in the present paper in order to propose possible analytical forms of the constitutive equations associated to the various behaviors. This is essentially a variant of a model proposed recently by Potanin [14]. It is also directly inspired by the image of the preferred mechanical paths transmitting the main forces in granular materials.

A. The system as an ensemble of resistant columns

At the very beginning, the system is made of fractal blobs of typical size $\xi \sim R_g$ (see Sec. II B.) connected together in a homogeneous network. Such a structure has clearly been found experimentally in the formation of a solid gel network [15]. When pressure is applied, the system rearranges irreversibly and the initial fractal blobs decrease in size as a consequence of local reorganization.

For the response to a stress, percolation is the appropriate description, since the mechanical resistance to collapse originates from a few paths made of bound particles, which span the top to the bottom of the system. These paths are formed as an assembly of blob backbones. These particular subsystems will be called the mechanically resistant columns (see Fig. 7). Since, for the mechanical response, two parallel independent columns are equivalent to one with double stiffness, we shall consider the case where there is only one such resistant column, the actual number of columns [16] being a numerical factor in the effective stiffness.

B. Stiff behavior

When the pressure is such that $P/P_o < 1$, the system is approximately elastic, as all relative displacements of particles remain quite small. For very small pressures, noncentral forces make the system rigid, preventing parts of the system from buckling [17]. Such a rigidity lasts until the pressure forces are strong enough to buckle the structure. Formally:

$$\phi = \phi_o, \quad \text{when } P < P_o. \tag{6}$$

In fact, the constraint $P < P_o$ is probably not so strict, and should be read as $P/P_o < A$, with the constant A of order 1. The important point here is that A should be independent of E_d, as bond ruptures are unlikely to occur.

C. Elastic behavior

When displacement of individual particles is allowed, but bond breaking is unlikely to occur because of the large value of the disruptive energy E_d, the system is a disordered elastic network. This corresponds to the conditions $1 < P/P_o < E_d/E_o$.

One could derive the response of the system by arguments based on the presence of resistant columns [18,14]. However, in this regime, the system is not yet markedly compressed, and one can expect structural effects due to the initial fractal morphology of the individual aggregates. This point is taken into account in the alternative derivation by Brown and Ball [19] for the homogeneous arrangement of disordered fractal clusters of finite size. This writes for the overall elastic modulus K_r of the system

$$K_r \propto \phi^{(3+x)/(3-D_f)}.$$

In this relation, the exponent x denotes the mass fractal dimension of the backbone of the aggregates of fractal dimension D_f. This leads to the elastic power-law behavior

$$P \propto \phi^{(3+x)/(3-D_f)}, \tag{7}$$

with the numerical estimate of the exponent: $(3+x)/(3-D_f) = 4.4 \pm 0.3$ for the reaction-limited cluster-cluster aggregates, in which $D_f = 2.1$ for the three-dimensional case. The relation (7) with a similar exponent (with a value 4–5) was also proposed with slightly different variations [20].

D. Ruptures

At a sufficient high pressure, bonds will start breaking, and the aggregates will no longer respond as an elastic system. Local rearrangements will cause the fractal structure to vanish rapidly. Since the volume fraction is now significantly higher than for the initial structure (say, about twice higher, or more), the initial fractal morphology has disappeared and one has to deal with a mechanical system equivalent to a single resistant column: the backbone of the percolation path spanning from the top to the bottom of the overall system. The density e of elastic energy stored in a column is $e = P^2/K_r$, where K_r coincides with the elastic modulus of the whole system. This density e corresponds to the deformation energy per unit volume.

From a mechanical point of view, only the minimal path crossing the backbone from top to bottom is relevant, since the loops renormalize the local stiffness throughout the path. This minimal path is then a self-avoiding walk. Two behaviors are possible.

1. Plastic behavior

The first behavior occurs when the elastic energy is distributed uniformly along the resistant column of height H. Rupture will occur if the applied pressure is larger than the threshold P^*_{pla} for which $e = w_o$, with w_o the average energy needed to break up all the bonds linking two neighboring

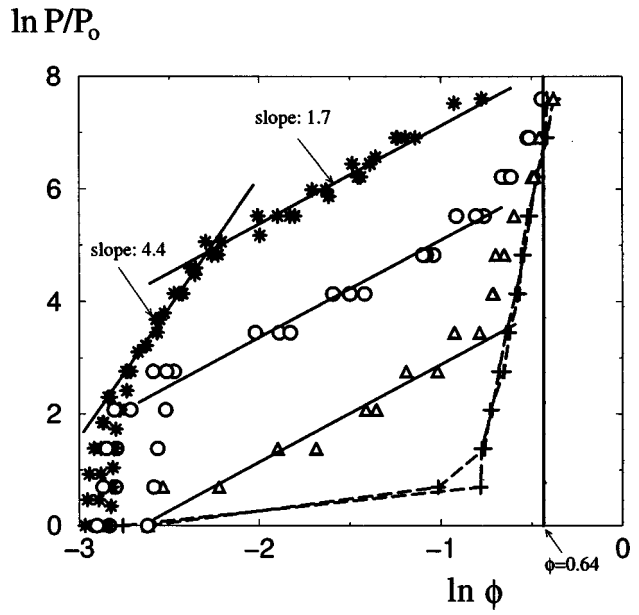

FIG. 8. A double-logarithmic plot of the reduced pressure P/P_o vs the volume fraction ϕ, for various values of the disruptive energy E_d. Triangles are for $E_d/E_o=4$, circles for $E_d/E_o=9$, and stars for various values of E_d/E_o ranging from 360 up to 10 000. A dashed line is used for the smallest values of E_d presented here: $E_d/E_o=0.04$, which exhibits discontinuous jump in ϕ from about 10^{-2} to 0.5 at $P/P_o \approx 1.25$. The latter is an example of fragile behavior (see text). Full straight lines (corresponding to power-law behaviors) are the predictions (7) and (9) of the theoretical model.

particles of the column [21]. Since $w_o \approx nE_d/a^3$ is independent on the volume fraction ϕ, one deduces the threshold: $P^*_{pla} \propto \sqrt{K_r}$.

The formula derived by Kantor and Webman for the effective stiffness of a disordered column is [18]

$$K_r = \frac{nka}{N_r R_\perp^2},$$

where n is the average number of springs between two neighboring particles, k is the stiffness of one bond, as discussed in Sec. II C, a the radius of one particle. At the denominator, N_r is the number of particles involved in the minimal chain throughout a percolating system. The scaling $N_r \propto H^{d_{min}}$ has been proposed with the numerical value $d_{min}=1.4$ for the three-dimensional space [22]. The distance $R_\perp$ was argued to follow a simple power-law $R_\perp \propto H^\epsilon$, with $\epsilon=1$ for the isotropic chains [14]. This leads to the dependence:

$$K_r \propto \phi^{2\epsilon+d_{min}}.$$

Therefore, one obtains the scaling relation:

$$P^*_{pla} \propto \phi^{\epsilon+d_{min}/2}. \quad (8)$$

The proportionality constant depends, in particular, on the value of E_d.

This formula needs an interpretation in terms of the current pressure P. This can be done by the following argument [3]. After a series of breakages, there is a collection of columns with all possible heights between 1 and H. When the external pressure reaches the threshold $P^*_{pla}(\phi)$ corresponding to the actual volume fraction through Eq. (8), then the resistant column of height H breaks into two or more fragments, and the volume fraction ϕ increases by the elastic deformation of the next resistant column. As this process goes on, the system passes successively through a series of discrete states $[P^*_{pla}(\phi), \phi]$. Between two consecutive states, the system evolves to equilibrium, first elastically, then through plastic deformation. But this transformation is not recorded, since only the equilibriium states are considered. If the disordered system is large enough, the states $[P^*_{pla}(\phi), \phi]$ are close to each other, and the behavior

$$P \propto \phi^{\epsilon+d_{min}/2} \quad (9)$$

is then expected, with the numerical exponent $\epsilon+d_{min}/2 \approx 1.7$ in the three-dimensional space.

2. Fragile behavior

The other behavior that involves column breakup, is that in which the deformation energy is localized into a small domain of the resistant chain. Then, the morphology of the

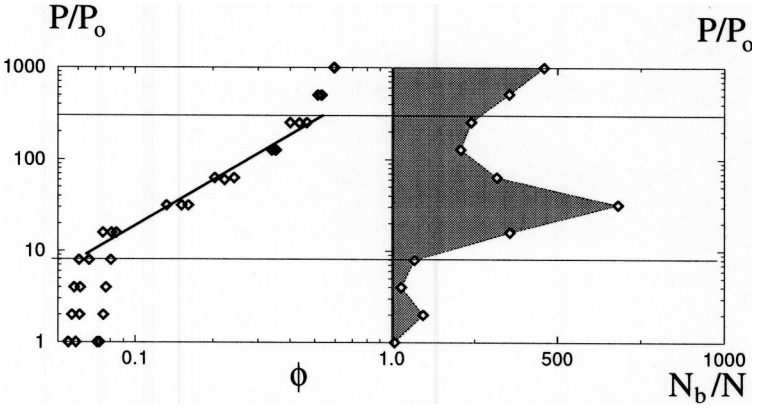

FIG. 9. The evolution of the breakage rate per particle N_b/N (right-hand figure) versus the pressure P/P_o, for three samples with $E_d/E_o=9$. The scale is linear in N_b/N, and logarithmic in pressure and volume fraction. The two horizontal lines visualize the boundaries of the plastic domain. The bold line is the slope 1.7.

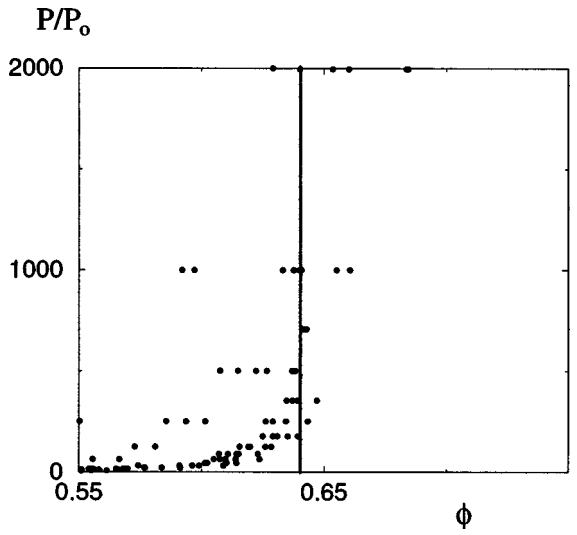

FIG. 10. A close view (domain: $0.55<\phi<0.75$) of the final compaction stages of the P vs ϕ curve in the double-linear plot, for all the numerical simulations performed in the current work (values of E_d/E_o ranging from 0.04 to 10000). The vertical solid line corresponds to $\phi^*=0.64$.

column does not matter, except in the vicinity of the stressed domain. The local breakage equation writes $P^*_{fra}a^3=w_o$, defining the pressure threshold P^*_{fra}. Since w_o is independent of the volume fraction ϕ, one concludes that this also applies to the pressure threshold. The expected behavior is quite different than previously: when pressure reaches the critical value P^*_{fra}, the system undergoes a series of breakups as in an avalanche, until the density ϕ becomes large enough to resist through lateral constraints. This will produce a discontinuity in the curve P versus ϕ at the value $P=P^*_{fra}$. Formally,

$$P \propto \phi^0 \quad \text{at} \quad P = P^*_{fra}.$$

E. Complete collapse

The bonds cannot resist the pressure forces whenever the pressure is larger than the threshold P^*_{dis} calculated in Eq. (5). Therefore, beyond P^*_{dis}, the system should be a compact arrangement of hard spheres. Because of the local randomness of the springs, one can expect the random close-packing model to be the final structure [23] if the system is able to overcome arch formation (as occurring in dry granular material). We infer

$$\phi = \phi^*, \quad \text{when} \quad P > P^*_{dis},$$

with $\phi^* \approx 0.64$ [24].

VI. NUMERICAL SIMULATIONS

A code was written in Fortran90, and numerical simulations performed on a 2.8 GHz biprocessor workstation. Typically, 20–50 CPU hours are needed for complete compaction of a system of 500 particles. Expect about one week for $N \sim 1000$.

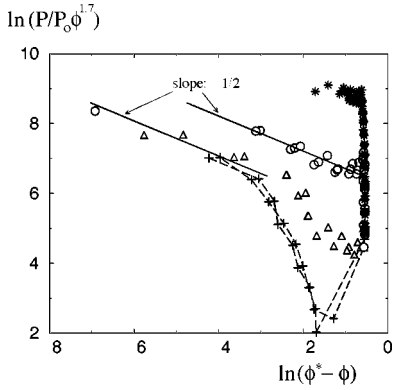

FIG. 11. Double-logarthmic plot of $P/P_o\phi^{1.7}$ vs $\phi^*-\phi$. The same data and the same symbols as for Fig. 8 are used. The lines of slope $-1/2$ could indicate the Van der Waals behavior (10) near the complete compact structure. The accumulated points in the right-hand side [close to $\ln(\phi^*-\phi)\sim-0.45$] correspond to the small volume fractions.

A. Numerical results

The main results of the present work are shown in Fig. 8. This is a double-logarithmic plot for the external pressure versus the volume fraction of the particles. Several sets of data are represented, all of them obtained from numerical simulations of systems with $N\approx 500$ particles, $n_t=200$ pins per particle, and $l_a=l_o$. Four sets of values of E_d were used, namely, $E_d/E_o=0.04$, $E_d/E_o=4$, $E_d/E_o=9$, and $E_d/E_o=360-10000$. The various behaviors are discussed and explained in the subsequent sections.

B. Stiff behavior

This behavior is not really important for our purpose, and it should correspond to the pressure domain P/P_o smaller than a constant independent on E_d, as explained in Sec. V B [see Eq. (6)]. The results plotted in Fig. 8 indicate that the stiff domain is well represented by $P/P_o<A$, with $A\simeq 7$ for all values of E_d.

C. Elastic behavior

This behavior can be seen only when the bonds cannot break so easily, i.e., for the large values of the disruptive energy E_d. In Fig. 8, for $E_d/E_o>360$ (stars), the power-law $P\propto\phi^{4.4}$ shows up over one decade in pressure. It corresponds precisely to the formula (7), when $1\ll P/P_o \ll E_d/E_o$. The remarkable feature of this part of Fig. 8 is that the detailed constitutive equation (with all its parameters, and domain of validity) is fairly independent on the relative disruptive energy E_d/E_o, as long as its value is larger than some threshold (here, larger than $\sim$100). This probably means that, in agreement with the theoretical argument of Brown and Ball [19], the full equation is essentially a function of the value of the local stiffness k of a spring, and of the morphology of the blobs.

D. Dissipative behaviors

1. Plastic behavior

As explained in Sec. V D, the plastic behavior is characterized by a series of breakages in a whole domain of pres-

sure. The theoretical feature is Eq. (9), which is precisely recovered in the numerical data of Fig. 8 as straight lines with slope 1.7. It is worth remarking that the same power-law equation fits well the data for different values of the disruptive energy, with a prefactor that increases with E_d. This suggests a common scenario yielding this behavior, as the one proposed in Sec. V D 1.

The role of the bond breakups is exemplified in Fig. 9, where it is seen that the pressure domain where plastic behavior occurs corresponds to a strong enhancement of the breakage rate (here counted as N_b, the total number of bonds broken between a given pressure and the previous equilibrated pressure).

2. Fragile behavior

For $E_d/E_o=0.04$, the bonds are so weak that the system cannot resist any pressure larger than a small threshold. This is basically a two-state system with no definite intermediate stable configuration in between the low-density initial state and the final compact state.

E. Collapse

All the numerical simulations tend to the finite volume fraction $\phi^* \approx 0.64$ of the random close-packing model, when the applied pressure is very high. This is seen in Fig. 10, which corresponds to the linear plot of all our data for which a limit value of ϕ was detected (the same data as Fig. 8 and other ones corresponding to various choices for the disruptive energy, the number N of particles and the number n_t of pins per particle). Only the domain $0.55<\phi<0.7$ is shown in order to clearly see the behavior.

The average value of the limit value is found equal to $\phi^*=0.643$, which is in close agreement with the value expected for the random close packing of spheres [25].

This is a remarkable result in the sense that it shows that presence of bonds between the particles forbids voids larger than those expected in the random close packing. One can say that springs here act as a lubricant, leading to a system definitely different from the dry granular medium at the same (i.e., here zero) temperature. In the latter system, the presence of arches and bridges may prevent the system from reaching the random close-packing state [26].

Close to the compact structure, compression should be dominated by the excluded volume effects. A tentative formula to describe the approach to the random close-packing result can be proposed here. Plotting the same data as in Fig. 8, but with the variables $(P/P_o)/\phi^{1.7}$ versus $\phi^*-\phi$, with $\phi^*=0.643$, in the double-logarithmic plot, one obtains Fig. 11. This plot exhibits a behavior, close to $\phi^*-\phi=0$, that resembles the Van der Waals equation (2), but in the modified form:

$$P/P_o \propto \phi^{1.7}/\sqrt{\phi^*-\phi}, \tag{10}$$

for all the data where the plastic behavior is clear (i.e., $1<E_d/E_o<100$). This formula is just indicative considering the small number of reliable points involved.

VII. CONCLUSION

The aim of this work was to determine the laws for the quasistatic compression of dissipative networks, made of aggregated particles that interact through noncentral forces. A model was constructed, which describes interparticle forces as breakable harmonic springs attached to the particle surfaces. The fundamental parameter of this model is the disruptive energy E_d needed to break one bond.

Numerical simulations of this model show a discrete set of compressional responses that are independent of initial conditions. Systems with low disruptive energies E_d respond with a plastic behavior, where large numbers of bonds are broken and created. Systems with higher disruptive energies respond with an elastic behavior, where most bonds are permanent. The scalings of pressure versus the volume fraction of particles in these two regimes can be understood through some general theoretical arguments. Finally, the numerical simulations also show that these scenarios converge, at very large applied pressures, to the random close packing of spheres.

This work may have practical uses in material sciences, for the design and the control of materials containing colloidal aggregates, such as ceramic pastes and flocculated emulsions. Indeed, the compressional properties of such materials are known from experiments that apply an osmotic stress, such as ultrafiltration, centrifugation, dialysis, or drying. There is strong evidence that the experimental laws are qualitatively similar to those predicted here. Typical examples can be found in Ref. [27] for compaction of dry colloidal silica, and Ref. [20] for polystyrene or colloidal alumina gels. A quantitative match of these laws would make it possible to determine the parameters that characterize interparticle forces, principally the bond strengths and the disruptive energies. Conversely, it is now possible to predict quantitatively the consequences of changes in interparticle forces for the mechanical properties of such materials.

ACKNOWLEDGMENTS

This work was supported by the French Ministère de la Recherche Scientifique, through the ACI Interface "Eau et Environnement." The authors thank Martine Meireles and Pierre Aimar for stimulating discussions and valuable comments.

[1] R. Jullien and R. Botet, *Aggregates and Fractal Aggregates* (World Scientific, Singapore, 1987).
[2] E.g., C. Goldenberg and I. Goldhirsch, Phys. Rev. Lett. **89**, 084302 (2002).
[3] R. Buscall and L. R. White, J. Chem. Soc., Faraday Trans. 1 **83**, 873 (1987).
[4] F. F. Lange and K. T. Miller, Am. Ceram. Soc. Bull. **66**, 1498 (1987); B. V. Velamakanni, J. C. Chang, F. F. Lange, and D. S. Pearson, Langmuir **6**, 1323 (1990); M. Colic, G. V. Franks, M. L. Fisher, and F. F. Lange, *ibid.* **13**, 3129 (1997).
[5] W. H. Shih, W. Y. Shih, S.-I. Kim, and I. A. Aksay, J. Am. Ceram. Soc. **77**, 540 (1994).
[6] P. A. Cundall and O. D.L. Strack, Geotechnique **29**, 47 (1979).
[7] Z. Zhou and B. Chu, J. Colloid Interface Sci. **146**, 541 (1991).
[8] V. Oles, J. Colloid Interface Sci. **154**, 351 (1992).
[9] D. A. Weitz, J. S. Huang, M. Y. Lin, and J. Sung, Phys. Rev. Lett. **54**, 1416 (1984).
[10] M. Tence, J. P. Chevalier, and R. Jullien, J. Phys. (Paris) **47**, 1989 (1986).
[11] R. Botet and P. Rannou, J. Phys. A **28**, 297 (1995).
[12] F. Radjai, D. Wolf, M. Jean, and J. J. Moreau, Phys. Rev. Lett. **80**, 61 (1998).
[13] L. Verlet, Phys. Rev. **159**, 98 (1967).
[14] A. A. Potanin, J. Colloid Interface Sci. **157**, 399 (1993); A. A. Potanin and W. B. Russel, Phys. Rev. E **53**, 3702 (1996).
[15] J. Bibette, T. G. Mason, Hu Gang, and D. A Weitz , Phys. Rev. Lett. **69**, 981 (1992).
[16] S. Havlin, in *Fractals in Physics*, edited by L. Pietronero and E. Tosatti (North-Holland, Amsterdam, 1986) p. 351.
[17] S. Alexander, Phys. Rep. **296**, 65 (1998).
[18] Y. Kantor and I. Webman, Phys. Rev. Lett. **52**, 1891 (1984).
[19] W. D. Brown and R. C. Ball, J. Phys. A **18**, L517 (1985).
[20] R. Buscall, P. D.A. Mills, J. W. Goodwin, and D .W.J. Lawson, J. Chem. Soc., Faraday Trans. 1 **84**, 4249 (1988); Wei-Heng Shih, Wan Y. Shih, Seong-Il Kim, Jun Liu, and Ilhan A. Aksay, Phys. Rev. A **42**, 4772 (1990); M. Chen, W. B. Russell, J. Colloid Interface Sci. **141**, 564 (1991); Hua Wu and M. Morbidelli, Langmuir **17**, 1030 (2001).
[21] S. O. Gregg, *The Surface Chemistry of Solids* (Chapman and Hall, London, 1965).
[22] J. Vannimenus, in *Physics of Finely Divided Matter*, edited by N. Boccara and M. Daoud (Springer, Berlin, 1985), p. 317.
[23] G. M. Channell, K. T. Miller, and C. F. Zukoski, AIChE J. **46**, 72 (2000).
[24] S. Torquato, T. M. Truskett, and P. G. Debenedetti, Phys. Rev. Lett. **84**, 2064 (2000).
[25] W. S. Jodrey and E. M. Tory, Phys. Rev. A **32**, 2347 (1985).
[26] L. A. Pugnaloni, G. C. Barker, and A. Mehta, Adv. Complex Syst. **4**, 289 (2001).
[27] F. Ehrburger and J. Lahaye, J. Phys. (France) **50**, 1349 (1989).